Research Square

Preprints are preliminary reports that have not undergone peer review.
They should not be considered conclusive, used to inform clinical practice,
or referenced by the media as validated information.

A Morphological Dual-Staining Framework for Standardized Detection of Cell Death in the Microalga Dunaliella salina

Mahnaz Barmshuri

m.barmeshuri@shirazu.ac.ir

Shiraz University

Saber Sadeghi

Shiraz University

Bahman Kholdebarin

Shiraz University

Zahra Faghih

Shiraz University

Laleh Ranjbaran

Shiraz University

Research Article

Keywords: Cell death, Dunaliella salina, MTT assay, iodine staining, apoptosis-like, necrotic, plasmolysis, and a novel secretion-type death

Posted Date: October 30th, 2026

DOI: https://doi.org/10.21203/rs.3.rs-11282227/v1

License: This work is licensed under a Creative Commons Attribution 4.0 International License.
Read Full License

Additional Declarations: No competing interests reported.

A Morphological Dual-Staining Framework for Standardized Detection of Cell Death in the Microalga *Dunaliella salina*

Mahnaz Barmshuri*, Saber Sadeghi, Bahman Kholdebarin, Zahra Faghih, Laleh Ranjbaran

Mahnaz Barmshuri:
E-mail address: barmshuribio@gmail.com and m.barmeshuri@shirazu.ac.ir
Postal address: Department of Biology, Faculty of Science, Shiraz University, Shiraz, Iran Postal Code: 7145685464

Saber Sadeghi:
E-mail address: ssadeghi@shirazu.ac.ir
Postal Address: Department of Biology, Faculty of Science, Shiraz University, Shiraz, Iran Postal Code: 7145685464

Bahman Kholdebarin:
E-mail address: bahmankholdebarin@gmail.com
Postal Address: Department of Biology, Faculty of Science, Shiraz University, Shiraz, Iran Postal Code: 7145685464

Zahra Faghih:
E-mail address: faghihz@sums.ac.ir
Postal address: Shiraz University of Medical Sciences, Shiraz, Iran; Postal Code: 3119-71345

Laleh Ranjbaran:
E-mail address: lalernjbrn@gmail.com
Postal address: Department of Biology, Faculty of Science, Shiraz University, Shiraz, Iran Postal Code: 7145685464

*** Correspondences:** barmshuribio@gmail.com and m.barmeshuri@shirazu.ac.ir

Highlights

1. Parallel MTT–iodine dual staining provides a reliable feature for distinguishing living from dead cells.

2. Necrotic, secretory, plasmolysis-type, and apoptosis-like cell death occur in Dunaliella salina.
3. We propose the establishment of a committee for the classification and nomenclature of cell death in unicellular aquatic organisms.

Abstract:

The absence of a simple, universal protocol to detect algal cell death is a major bottleneck in aquatic ecology and carbon cycle research. This study bridges this gap by establishing a practical diagnostic framework based on parallel 3-(4,5-dimethylthiazol-2-yl)-2,5-diphenyltetrazolium bromide (MTT) and iodine staining, concurrently probing the two pillars of photoautotrophic vitality—metabolic activity (via respiratory electron transport) and photosynthetic storage integrity. Using the halotolerant, wall-less model *Dunaliella salina*, we applied the method to environmentally relevant stressors. It clearly distinguished viable cells and consistently classified four distinct death phenotypes: apoptosis-like, necrotic, plasmolysis, and a novel secretion-type death from microbial fouling. Notably, light-induced necrosis exhibited morphological hallmarks of singlet oxygen-mediated killing, analogous to Type II Photodynamic Therapy. Crucially, identical death signatures were detected in natural populations from Maharloo Hypersaline Lake, confirming ecological validity. Beyond providing a robust, field-adaptable toolkit, our findings expose a critical disciplinary gap: the lack of standardized nomenclature and diagnostic criteria for cell death in carbon-fixing unicellular organisms. As these organisms mediate nearly half of global carbon fixation, quantifying their mortality is essential for improving carbon fixation and growth models, accurately predicting carbon fluxes, assessing the resilience of aquatic carbon sinks, and evaluating climate change impacts. We therefore propose an international consortium on Cell Death in Carbon-Fixing Unicellular Organisms to standardize definitions of cell death phenotypes, unify methodologies through this dual-staining protocol, explicitly incorporate mortality into carbon fixation and growth models, and translate laboratory-based viability metrics into predictive tools for ecosystem- and photobioreactor-scale carbon management. Our framework provides the essential methodological foundation for this global standardization effort.
Keywords: Cell death; *Dunaliella salina*; MTT assay; iodine staining; apoptosis-like; necrotic; plasmolysis; and a novel secretion-type death

Introduction:

Green algae play essential roles in the dynamics and structure of marine food webs, the biochemical carbon cycle, and the cycling of bio-limiting elements in marine environments (Finkel et al. 2010). It has been demonstrated that certain eco-physiological processes of green algae in marine ecosystems influence both their mortality and the mode of cell death (Bidle 2015). Evidence has been presented indicating that various factors affect the controlled degradation of green algae, with different forms of cell death described as algal responses to biotic and abiotic stresses (Segovia et al. 2003; Franklin et al. 2006; Darehshouri et al. 2008; Jimenez et al. 2009;

Yordanova et al. 2013). As observed in leading studies, definitive detection of cell death in microalgae relies on complex multifaceted approaches such as membrane integrity assays, caspase-like activity measurements, reactive oxygen species (ROS) detection, chlorophyll fluorescence analyses, and ultrastructural observations (Gao and Erdner 2022; Gachon et al. 2025). Nevertheless, dead algal cells may retain chlorophyll autofluorescence after irreversible cell death, leading to their misidentification as viable cells and potentially biasing estimates of phytoplankton mortality and carbon cycling.

Accurate and early identification of algal cell death is critical for improving the reliability and accuracy of carbon cycle models and growth dynamics in aquatic systems, particularly under climate change–driven shifts in temperature, ocean acidification, and light regimes that can significantly alter phytoplankton physiology and mortality patterns. It is also essential for maintaining stable production in photobioreactor-based cultivation systems, where it supports more reliable estimation of growth dynamics, improved process optimization, and prevention of culture collapse.

Based on this need, we hypothesize that a dual-staining approach targeting both respiratory metabolic activity and photosynthetic integrity can provide a rapid and reliable proxy for distinguishing viable, stressed, and non-viable algal cells, thereby enabling early detection of population-level decline before irreversible culture collapse occurs.

Materials and Methods

Cell Groups and Experimental Design

To evaluate the capability of the proposed morphological staining method for detecting cell death across a spectrum of conditions, cells from four distinct groups were analyzed:

1: Natural cells from Maharloo Hypersaline Lake: This group served as an environmental benchmark, containing cells subjected to combined natural stresses (salinity levels of up to 350 g L^{-1} sustained for 4–8 months, cell suspension temperatures of 60–65 °C for approximately 5 hours per day, and severe light stress).

2: Sedimented cells from aged laboratory cultures (9 months): This group represented a model of chronic nutrient deprivation. Previous studies have linked long-term culture aging and nutrient depletion to programmed cell death (PCD) in microalgae (Berman-Frank et al. 2004). Cell death in this group occurred spontaneously during prolonged cultivation under chronic nutrient deprivation, together with cell sedimentation and the accumulation of extracellular secretions, which likely increased the apparent viscosity of the culture medium and may have contributed to the formation of a stressful and potentially toxic microenvironment.

3: Cells treated with Cisplatin: This group acted as a positive control for induced apoptotic-like death. Cisplatin, a DNA-alkylating agent, triggers programmed cell death pathways via DNA cross-linking (Bidle 2015).

4: Cells exposed to high-intensity visible light: This treatment was designed to induce acute photo-oxidative stress. Excessive light leads to reactive oxygen species (ROS) overproduction in chloroplasts, capable of inducing both necrotic and programmed cell death (Murik et al. 2014). The salinity level in cell groups two to four was 116 g L^{-1}.

Habitat and Collection Site of *Dunaliella. salina*

Dunaliella salina cells were collected from Maharloo Hypersaline Lake (MHSL), a hypersaline lake located approximately 23 km east of Shiraz, Iran (geographical coordinates: 29°29'29" N, 52°44'17" E to 29°19'21" N, 52°54'32" E). The lake spans an area of about 250 km² (Fig. 1). Its physicochemical characteristics have been previously documented (Zamanpoore et al. 2019).

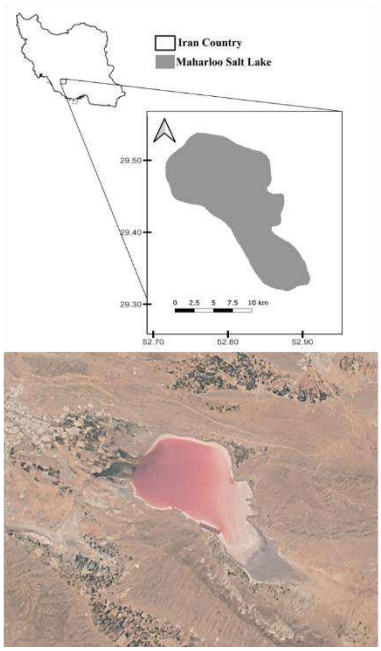


Fig. 1 Geographical location of MHSL in Iran (left). Aerial photograph of MHSL taken from the NASA International Space Station in 2015 (right)

Identification of *D. salina* and Culture Conditions

D. salina was identified based on morphological keys (Borowitzka & Siva 2007; Borowitzka 2018). Lake-collected cell suspensions were transported to the laboratory and maintained at 25 ± 1°C under a light intensity of 40–50 µmol photons m^{-2} s^{-1} (cool white fluorescent lamps) with a 16:8 h light:dark photoperiod (Xu et al. 2016). The salinity level in cell groups two to four was 116 g L^{-1}.

The concentrations of the compounds in the *Dunaliella* culture medium are as given in Table 1.

Table. 1 Concentrations of compound in the culture medium

Compound	Final Concentration	Unit
$MnCl_2$	7	μM
EDTA	5	μM
$FeCl_3$	2	μM
$ZnCl_2$	1	μM
$CuCl_2$	1	μM
$CoCl_2$	1	μM
$(NH_4)_6Mo_7O_{24}$	1	μM
$NaHCO_3$	50	mM
$MgSO_4$	5	mM
KNO_3	0.75	mM
KH_2PO_4	0.2	mM
$CaCl_2$	0.2	mM
NaCl	2	M

Experimentally Induced Cell Death

Cisplatin Treatment

To establish definitive criteria for cell death, we induced apoptosis-like death using cisplatin (Sobhan Oncology, 1 mg mL^{-1}). Cells in the mid-logarithmic growth phase were used. Aliquots of 100 μL cell suspension (1×10^5 cells mL^{-1}) were placed in microtubes. Cisplatin (1 μg mL^{-1}) was added to achieve final volumes of 25, 50, 75, and 100 μL per tube. The total volume was adjusted to 200 μL with cell-free medium. A control group received 200 μL of cell suspension without cisplatin. For each concentration, 18 replicates were prepared: nine were incubated for 24 h and nine for 48 h in darkness at 37°C, with lids sealed to prevent evaporation. Post-incubation, cells were assessed for damage via iodine and 3-(4,5-dimethylthiazol-2-yl)-2,5-diphenyltetrazolium bromide (MTT)staining.

Visible Light Irradiation:

Cell death was also induced by photo-oxidative stress using an Olympus BX61 microscope light source equipped with a BA590 barrier filter and DM570 dichroic mirror. For 25 replicates, 200 μL of cell suspension (1×10^5 cells mL^{-1}) was placed on a glass slide (24 × 60 mm), covered, and irradiated at multiple fields for 2-minute intervals. After irradiation, slides were rinsed with cell-free Ben-Amotz medium (Ben-Amotz et al. 1989). Cells were then collected by centrifugation (3,000 rpm, 1 min), resuspended in 2 mL of fresh medium, and transferred to a 96-well plate for staining. The timing of death in vegetative cells and zygotes was recorded.

Assessment of Cell Viability and Morphology:

MTT Reduction Assay

Cellular metabolic activity was assessed using the MTT assay. Following cisplatin treatment, 10 μL of MTT solution (10 mg mL^{-1} in PBS) was added to each microtube and incubated for 4 h at

37°C (lids sealed). Cell-free medium served as the blank. For quantification, samples were centrifuged (3,000 rpm, 5 min), the supernatant was discarded, and the pellet was resuspended in 200 µL DMSO. After 5 min at room temperature and vortexing, samples were centrifuged again (6,000 rpm, 10 min) to pellet debris. The violet supernatant was transferred to a 96-well plate, and absorbance was measured at 570 nm using a POLARstar Omega plate reader (BMG Labtech). In parallel, pure *D. salina* cultures and environmental samples from Maharloo Lake (1×10^4 cells mL^{-1}) were treated with 10 µL MTT and incubated for 24–144 h (6 replicates per time point) to compare metabolic activity over time.

Microscopic Staining and Morphological Analysis:

MTT Staining for Metabolism: Cellular morphology and intracellular formazan crystal formation were examined across all groups using an Olympus BX61 light microscope. **Iodine Staining for Pyrenoid/Starch:** An iodine reagent (0.3 g KI + 0.15 g I_2 in 50 mL distilled water) was used. Gradually, 2 µL of reagent was added to 400 µL cell suspension (1×10^5 cells mL^{-1}) until a dark violet endpoint (with visible cell precipitation) was reached. A drop of the stained suspension was smeared on a slide and examined under the same microscope.

Results

Impact of Cisplatin on Cell Viability and Morphology

To establish definitive criteria for cell death, the effects of various cisplatin concentrations and exposure times on the viability and morphology of *D. salina* cells were assessed. Dose-response analysis (Fig. 2a) confirmed the cytotoxic effect of cisplatin, with half-maximal inhibitory concentration (IC_{50}) values of 0.75 mM at 24 hours and 0.16 mM at 48 hours. These results demonstrate a dose- and time-dependent reduction in cell viability. Increasing cisplatin concentration progressively decreased MTT reduction at both time points, and the effect was more pronounced after 48 h, as reflected by the lower IC_{50} value (0.16 mM) compared with 24 h (0.75 mM). This indicates that prolonged exposure enhanced the cytotoxic effect of cisplatin. Statistical analysis using multiple t-tests (one per row) in GraphPad PRISM 9 revealed that the increase in MTT reduction potential over time was significant ($p < 0.05$). Notably, although the same initial cell number was used in the control group (0 mM cisplatin), significant differences in MTT reduction were observed between the 24- and 48-hour time points (Fig. 2b).

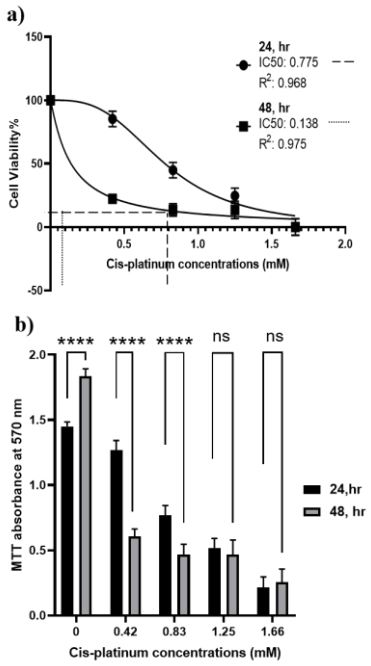


Fig. 2 Effect of cisplatin on *D. salina* cell viability and metabolic activity. **(a)** Dose-response curves of *D. salina* cell viability following 24-h (black bars) and 48-h (gray bars with black outline) exposures to various cisplatin concentrations, as determined by MTT assay. The half-maximal inhibitory concentration (IC_{50}) and the coefficient of determination (R^2) for each curve are indicated

(b) MTT reduction potential (absorbance at 570 nm) of *D. salina* cells after 24 and 48 hours of exposure to the indicated cisplatin concentrations. Data are presented as mean ± standard deviation (SD) (n = 3). Statistical significance between the control (0 mM) and cisplatin-treated groups was determined using multiple t-tests

Higher absorbance values indicate greater MTT reduction, reflecting higher photosynthetic electron transport activity and, consequently, a healthier photosynthetic system (Increased MTT reduction corresponds directly to a higher ratio of viable cells, whereas decreased absorbance values are attributable to attenuated metabolic turnover and cellular death).

Comparative MTT Reduction in Pure versus Environmental Samples

In a separate experiment, the MTT reduction potential was compared between pure laboratory cultures of *D. salina* and mixed cell suspensions collected directly from MHSL over a 144-hour period (Fig. 3)

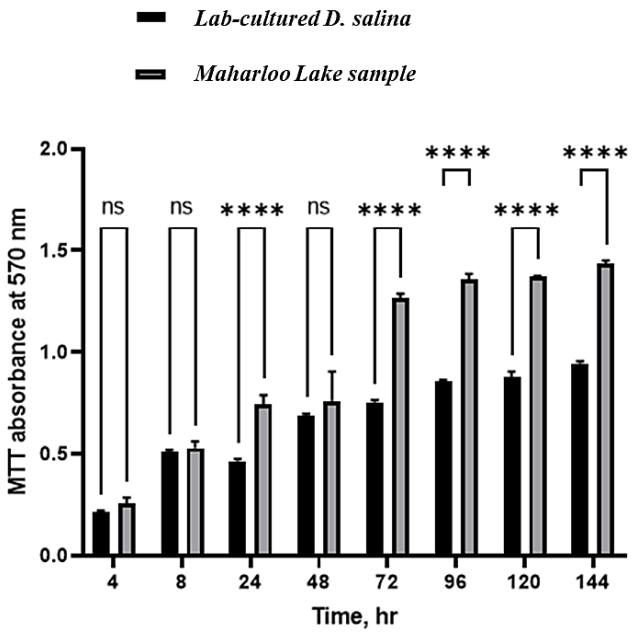


Fig. 3 Time-dependent MTT reduction in laboratory-cultured versus environmental *D. salina* suspensions.

Despite using equal initial cell densities (1×10^4 cells mL^{-1}), the cell suspensions prepared directly from MHSL exhibited significantly higher absorbance values and more intense color formation due to formazan crystals compared to the pure laboratory cultures of *D. salina* (Fig. 3). Microscopic analysis revealed that the environmental samples contained a diverse community of microorganisms (including ciliates, amoebae, and other microbes), all capable of reducing MTT
In contrast, the laboratory-maintained cultures harbored far fewer such contaminating populations. This finding confirms that the elevated MTT reduction signal in natural samples reflects the **total metabolic activity of the entire microbial consortium**, not solely that of *D. salina*

Morphological Criteria for Distinguishing Viable and Non-Viable Cells

A combination of MTT and iodine staining was employed to establish clear, reliable morphological markers for differentiating between living, dead, and dying *D. salina* cells. The MTT stain localizes to active metabolic sites within viable cells, while iodine specifically targets the starch grains surrounding the pyrenoid. These distinct staining patterns revealed consistent and diagnostic differences in cellular architecture.

These two staining methods are incompatible with each other, and both stainings must be performed independently. Iodine staining disrupts the metabolic activity of the cell, so MTT is not reduced because oxidoreductase activity is halted. On the other hand, reduction of MTT by oxidoreductase produces formazan crystals throughout the living cell and prevents visualization of the starch granules around the pyrenoid.

When is a cell alive?

The definitive morphological criteria for identifying living *D. salina* cells—based on flagellar presence, chloroplast integrity, pyrenoid structure, and specific staining patterns with both iodine and MTT—are systematically detailed in Table 2 and Fig. 4.

Table 2. Key morphological features distinguishing living *D. salina* cells under different staining conditions

Diagnostic Feature	Observation in Untreated Living Cells	Observation after Iodine Staining	Observation after MTT Staining	Notes on Cell State / Cycle
Flagella	Two actively moving flagella.	Two non-motile flagella visible.	Two non-motile flagella visible; MTT reduction occurs at flagella.	Palmelloid/non-flagellated stages exist during asexual reproduction. Four flagella appear during early sexual reproduction (protoplast conjugation).
Cell Shape & Outline	Typical egg-shaped cell.	Egg shape maintained; often shows bubble formation around the cell membrane.	Egg shape maintained.	–

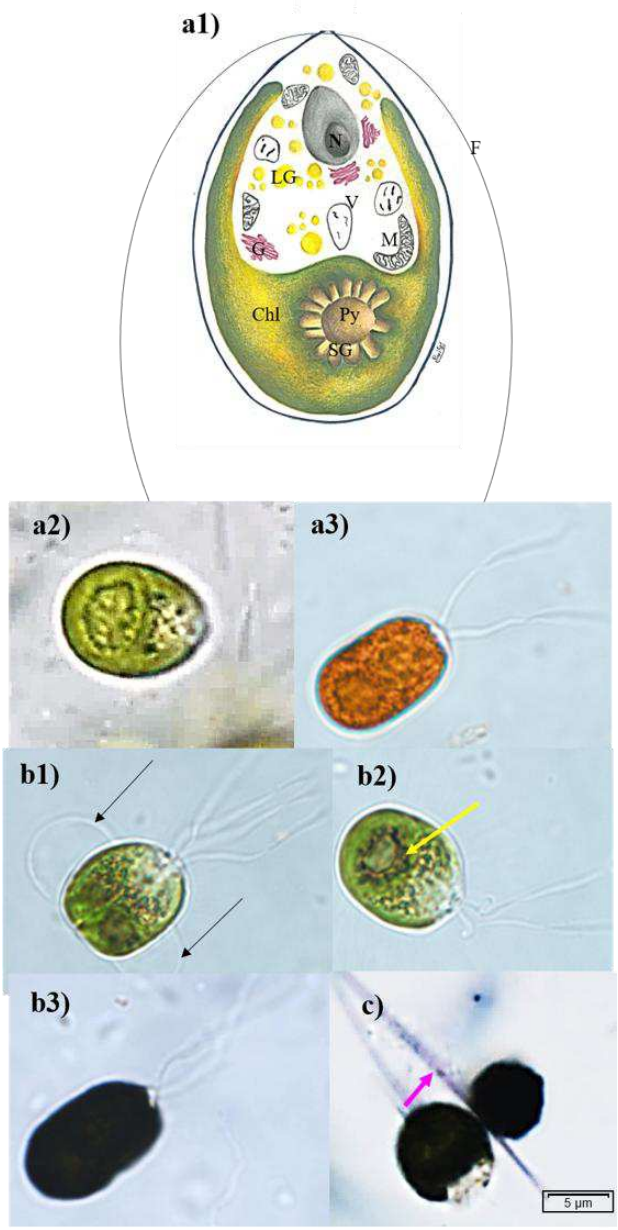


Fig. 4 General morphology of living *D. salina* cells under various conditions and staining methods

(a) Schematic illustration of a *D. salina* cell. Key structures are labeled: **F,** flagella; **N,** nucleus; **LG,** lipid globules; **V,** vacuole; **M,** mitochondria; **Chl,** chloroplast; **Py,** pyrenoid; **SG**, starch grains **(a2)** Typical green *D. salina* cell in standard condition **(a3)** Cell under salinity stress showing accumulated beta-carotene (orange coloration) **(b1)** Early stage of hologamy (sexual reproduction via protoplast conjugation). The cell exhibits four flagella, two pyrenoids, and membrane bubbles formed after iodine treatment (black arrows) **(b2)** Iodine staining of a green

cell, highlighting the starch grains surrounding the pyrenoid (yellow arrow) **(b3)** Iodine staining of a cell containing beta-carotene. The direct correlation between beta-carotene and starch content is evident. This staining approach is recommended for determining the optimal harvest time for beta-carotene extraction in commercial *D. salina* cultures **(c)** MTT staining of a living cell. Reduction of MTT occurs throughout the entire cup-shaped chloroplast. Needle-shaped formazan crystals have been dislodged from the cell (purple arrow).

When is a cell dead?

Following the conceptual framework of the Nomenclature Committee on Cell Death (NCCD), which distinguishes between the *process* of dying and the *endpoint* of death (Kroemer et al. 2009), we defined cell death in *D. salina* as the irreversible point-of-no-return. In this photosynthetic microalga, we posit that catastrophic damage to the photosynthetic apparatus—the cell's most vital system—halts photosynthesis and commits the cell to death. This terminal state manifests through distinct, observable morphological alterations. Based on our experimental observations, cell death in *D. salina* was categorized into four distinct types. The defining morphological characteristics for each type are systematically detailed in Table 3.

Table 3. Classification and morphological characteristics of cell death in *D. salina*.

Type / Inducer of Cell Death	General Cell Morphology	Iodine Staining (Pyrenoid/Starch grain) (Borowitzka& Siva 2007; Borowitzka 2018)	MTT Staining (Metabolic Activity)	Corresponding Panel in Fig. 5
Cisplatin-induced death	Ovoid-shaped cell with two non-motile flagella.	Slight staining of starch grain around pyrenoid.	Uneven and faint staining of the chloroplast.	A
Visible Light-induced necrosis	Ovoid-shaped cell, no flagella. Cell ruptured/disintegrated from the anterior region.	No staining of starch grains.	No staining of metabolic sites.	B
Environmental necrosis (Maharloo Lake sample)	Green, ovoid-shaped cell without flagella. Disintegrated from the anterior side.	No staining of starch grains.	No staining of metabolic sites.	B
Plasmolysis-type death (Advanced)	Ovoid-shaped to spherical deformed, no flagella. Membrane completely detached from cell wall (plasmolyzed).	Irregular starch sheath present around pyrenoid.	No staining of metabolic sites.	C
Plasmolysis-type death (Partial/Depression)	Ovoid-shaped to spherical deformed, no flagella. Local depression or partial membrane detachment.	Irregular starch grain's structure present.	No staining of metabolic sites.	C
Secretion-type death (Sediment of old culture)	Spherical deformed, compressed cell, no flagella. Lipid droplet exudation. Signs of infection.	Starch grain present around compressed pyrenoid	No staining. Internal infection often observed.	D

A Microscopic Gauge of Algal Mortality

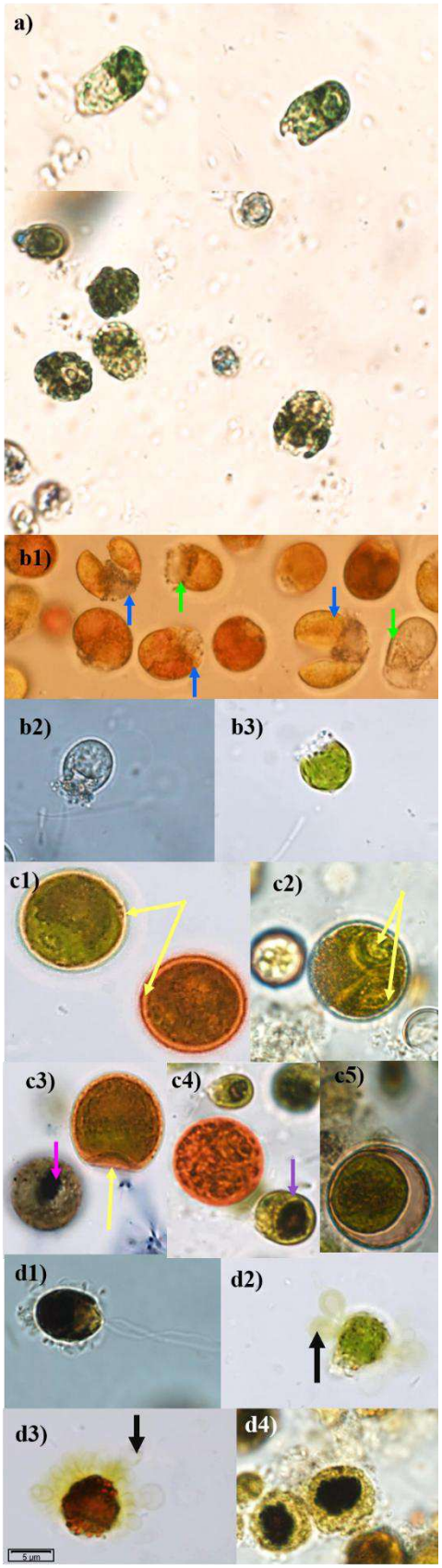


Fig.5 Morphological classification of cell death types in *D. salina*.
(a) Representative image of *D. salina* cells treated with cisplatin, showing dead cells as indicated by the absence of MTT reduction.
(b) Necrosis induced by visible light. **(b1)** Single cell undergoing light-induced necrotic death. The cell shows rupture at the anterior region with leakage of cellular contents (green arrow). Necrotic death in two fused cells (blue arrows); fusion is not yet complete, and during light stress the cells rupture from the posterior region. See Supplementary Video 2 and 3 for the complete process of this death type. **(b2)** Loss of pigmentation (bleaching) following prolonged irradiation **(b3**) Necrotic cell observed in environmental samples from Maharloo Lake
(c) Plasmolysis-type cell death (negative MTT reduction) **(c1)** The onset of plasmolysis during cytokinesis is marked by initial membrane–cell cover separation (yellow arrow) **(c2)** Cytokinesis with two daughter cells undergoing plasmolysis is shown, with two pyrenoids indicated by yellow arrows **(c3)** Surface indentation at early plasmolysis (yellow arrow) is likely caused by residual membrane attachments to the cell cover pulling inward during cytoplasmic shrinkage following loss of osmotic potential. : intracellular infection detected by MTT staining (pink arrow) : The oval-shaped peripyrenoidal starch grain pattern likely reflects pyrenoid degradation under intracellular or environmental stress (purple arrow) **(c4)** Complete plasmolysis with full membrane–cell cover detachment is clearly visible.
(d) Secretion-type cell death **(d1)** Microbial attachment to an algal cell (iodine-fixed) **(d2-d3)** Osmotic imbalance, cellular depression, and lipid droplet exudation (black arrows) due to microbial infection **(d4)** Compression of the pyrenoid structure.
(For a systematic classification and detailed morphological criteria of each death type, see Table 3)

Discussion

In this study, we observed multiple morphologically distinct outcomes in *D. salina* populations under stress, including apoptosis-like, necrotic, secretory, and plasmolysis-type cell death. These outcomes share morphological features with each other and with normal growth and division processes, which may lead to misinterpretation without careful time-resolved observation. Here, we discuss the criteria that distinguish these processes and the implications of our findings for the interpretation of cell death in *Dunaliella* Table 3.

3.1. A Dual-Staining Approach to Define Life and Death in a Photosynthetic Cell.

The fundamental challenge in microalgal cell death research lies in the lack of simple, universal criteria to unequivocally distinguish living from dead cells. It should be noted that photosynthesizing cells exhibit two types of fluorescence: chlorophyll autofluorescence and functional photosynthetic fluorescence. Following cell death, the cessation of photosynthetic electron transport and the loss of metabolic activity leave only chlorophyll autofluorescence, which persists until complete chlorophyll bleaching. This residual signal should not be equated with the functional fluorescence of the photosynthetic system. Furthermore, the peripyrenoidal starch grain

storage pattern in living cells follows a distinct pattern that changes in dead cells. Therefore, to determine the definitive characteristics of cell death, it is necessary to assess both the metabolic activity of the cell and its starch storage pattern. Moving beyond the evidence presented in earlier studies on unicellular aquatic organisms (Segovia et al. 2003; Bidle 2016; Aguilera et al. 2021), we developed a composite morphological definition of cell death based on two pillars of photosynthetic vitality: (i) metabolic activity, assessed by MTT reduction and functional photosynthetic fluorescence, and (ii) the pyrenoid starch grain storage pattern, which is distinct in living cells and altered in dead cells. with recent studies highlighting critical considerations for its application (Ghasemi et al. 2021; Carreno et al. 2021)—and iodine staining, which targets the starch grain of the pyrenoid. The pyrenoid is no longer viewed merely as a static protein aggregate but as a dynamic, phase-separated organelle central to the CO_2-concentrating mechanism (Rosenzweig et al. 2017; Barrett et al. 2021). By applying these stains separately and integrating their readouts, we could independently probe the integrity of the photosynthetic electron transport chain (via oxidoreductase activity reflected in MTT reduction) and the functional output of the Calvin cycle (via starch deposition). This integrated approach provides a robust, binary, and functionally informative assessment of cell viability (Tables 2 & 3, Figs. 4 & 5).

Chemically-Induced, Apoptosis-Like Death.

Cisplatin, a canonical DNA-damaging chemotherapeutic agent known to induce intrinsic apoptosis through DNA damage and mitochondrial perturbation (Galluzzi et al. 2012), served as our positive control. Our observation of reduced MTT reduction aligns with its established role in disrupting mitochondrial electron transport and amplifying reactive oxygen species (ROS) production (Yang et al. 2006; Liu et al. 2025; Brown et al. 2019). In photosynthetic eukaryotes like *D. salina*, the mechanisms of cisplatin toxicity likely extend beyond the nucleus. Given the prokaryotic origin and semi-autonomous nature of chloroplasts, we propose that cisplatin may also interact with the chloroplast genome or transcriptional machinery, analogous to its effects on mitochondrial DNA (Podratz et al. 2011; Kleih et al. 2019). Such targeting could specifically inhibit the expression of photosynthetic oxidoreductases, which are crucial for both linear and cyclic electron flow. This dual attack on mitochondrial and chloroplastic bioenergetics would catastrophically compromise ATP/NADPH synthesis and the cellular reducing power necessary for MTT conversion, mechanistically explaining the faint and uneven metabolic staining we observed in cisplatin-treated cells (Fig. 5a, Table 2). This apoptosis-like phenotype in *D. salina* contributes to the growing body of evidence for conserved programmed cell death (PCD) pathways in unicellular photosynthetic eukaryotes (Bidle 2016).

Light-Induced Necrosis and its Environmental Echo: Evidence from Dynamic Imaging and Modern Photobiology

A pivotal finding was the induction of necrotic death by visible light in the lab and the observation of morphologically identical dead cells in MHSL (Fig. 5b). This paradox—where the essential

energy source for photosynthesis becomes a lethal agent—can be explained by a well-characterized photochemical cascade that our real-time imaging directly captures.

Under the high-intensity, focused light of our microscope, the photon flux exceeds the photosynthetic capacity, leading to severe photosystem II (PSII) photoinhibition and the over-reduction of the electron transport chain (ETC), a well-documented bottleneck under excess light (Orf et al. 2022). Our time-lapse video evidence (Video V1) provides direct visual proof of this initial failure: the expected rapid quenching of chlorophyll fluorescence—a hallmark of regulated photoprotection via non-photochemical quenching (NPQ)—is conspicuously absent. Instead, the excess excitation energy in the light-harvesting complexes promotes the formation of the long-lived, highly reactive chlorophyll triplet state (^{3}Chl) from the singlet excited state (^{1}Chl).

The fate of ^{3}Chl is critical. In healthy cells, carotenoids like beta-carotene efficiently quench ^{3}Chl, preventing damage (Telfer 2002). However, under sustained high light, this protective system can be saturated, as the rate of ^{3}Chl formation exceeds the quenching capacity (Niyogi and Truong 2013). The ensuing reaction between ^{3}Chl and ground-state oxygen ($^3O_2$) generates cytotoxic singlet oxygen ($^1O_2$) predominantly at PSII, a primary site of photo-oxidative damage (Dogra and Kim 2020; Krieger-Liszkay et al. 2008). $^1O_2$ is a potent signaling molecule and executioner, initiating lipid peroxidation, oxidizing proteins (notably the D1 protein of PSII), and causing irreversible damage to cellular membranes (Dogra and Kim 2020; Exposito-Rodriguez et al. 2017). The visible consequence is rapid cellular bleaching (Fig. 5b2), as photosynthetic pigments are destroyed.

The culminating necrotic rupture was captured in real-time. Video V2 and V3 reveals the sequence: following the photo-oxidative burst, a sudden contraction of the cell from the anterior pole occurs, culminating in catastrophic membrane rupture. We propose this is a direct result of $^1O_2$-mediated massive lipid peroxidation in the chloroplast and plasma membranes, coupled with the breakdown of osmotic homeostasis. This process is mechanistically analogous to the membrane permeabilization and bleb formation observed in Type II (oxygen-dependent) Photodynamic Therapy (PDT), where a photosensitizer generates $^1O_2$ to kill cancer cells (Kwiatkowski et al. 2018; Lan et al. 2019). In our case, chlorophyll itself acts as the endogenous photosensitizer.

This laboratory-defined mechanism provides a plausible explanation for the environmental necrosis observed in MHSL. We hypothesize that under specific atmospheric conditions, salt crusts and halite crystals—whose formation and persistence are well-documented in hypersaline environments (Orr 2017)— These crystalline structures may act as transient optical elements at the lake surface, potentially concentrating incoming solar radiation and generating localized zones of elevated irradiance. A similar stress scenario can be observed in polar environments, where melting ice exposes previously shaded microalgal communities to abrupt and intense increases in light stress. In hypersaline systems, episodic formation of salt pans followed by rainfall or seasonal

hydrological disturbances may resuspend previously shaded cellular suspensions and transport them to the surface, where they become suddenly exposed to high solar irradiance. In natural samples, we observed cells that we attribute to light stress. These cells maintained their overall morphology, and flagella were occasionally still present. Notably, iodine staining revealed a pyrenoid starch grain pattern similar to that of living cells. Based on these features, we designated them "frozen cells" (Fig. 6). These cells are presumably viable and may be capable of restoring maximal metabolic activity upon chlorophyll recovery. Such rapid transitions could trigger photo-oxidative stress and contribute to necrotic cell death pathways comparable to those induced under controlled laboratory conditions.

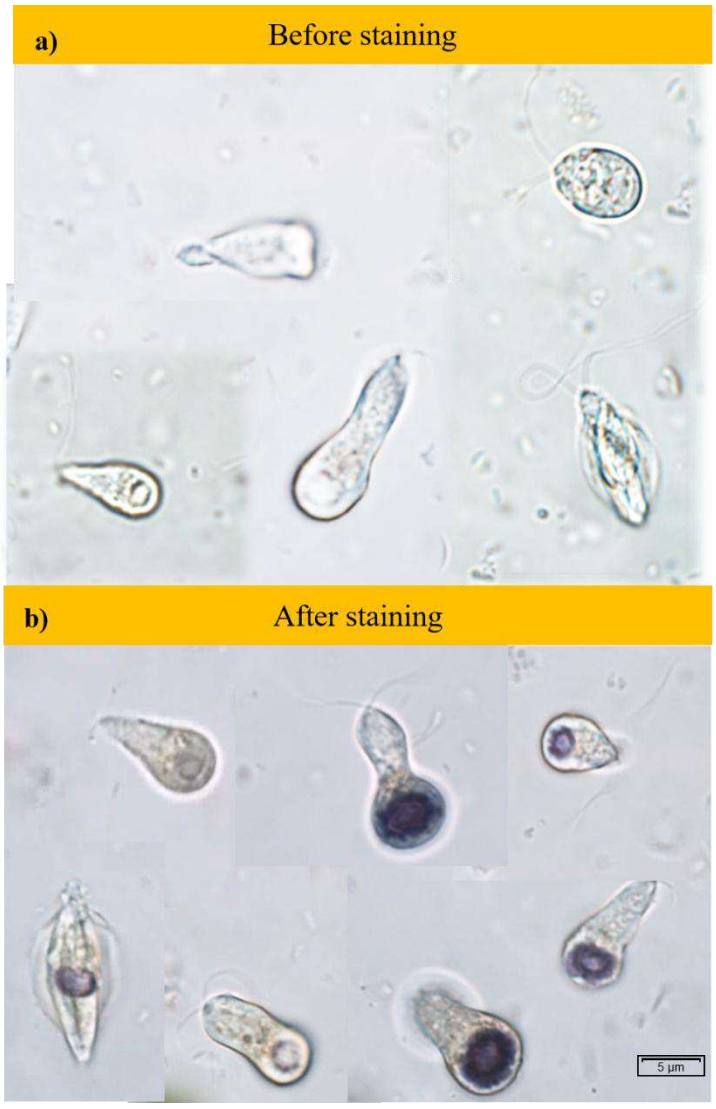


Fig. 6 Salt-Frozen Cells were observed in a cell suspension with a salinity exceeding 5.5 M during the peak of the drought period **(a)** Salt-Frozen Cells before pyrenoid starch grain with iodine reagent **(b)** Salt-Frozen Cells after starch grain staining with iodine reagent

Finally, Video S1 recorded a telling optical signature: a transient post-mortem phosphorescence emitted immediately after bleaching ceased. This faint afterglow likely originates from the delayed radiative decay of triplet states or altered pigments within the irreversibly damaged photosynthetic apparatus (Krieger-Liszkay et al. 2008) serving as a direct spectral fingerprint of the terminal photo-oxidative cascade.

Plasmolysis-Type Death in Sedimented, Growth-Arrested Cells.

To better understand the distinction between cytokinesis and aplanospore formation, we describe here the unique features of each process in detail.

Distinguishing Cytokinesis from Aplanospore Formation

Under normal growth conditions, *D. salina* divides by longitudinal fission, producing two flagellated daughter cells. Under stress conditions, however, cells may enter multiple fission (palintomy), producing 2^n daughter cells within the mother cell cover. These daughter cells may be released as motile cells (zoospores) or as non-motile cells (aplanospores or autospores). The distinction between these outcomes is critical: cell division represents ongoing proliferation, whereas aplanospore formation represents a survival strategy under adverse conditions (Borowitzka & Siva 2007; Borowitzka 2018).

In our documenting through photos and video, we observed that daughter cells remained enclosed within the mother cell membrane after release from the cell cover (see Supplementary Video and Figures). This observation suggests that the cell cover and plasma membrane are structurally and functionally distinct, and that the mother cell membrane is retained during cytokinesis. To our knowledge, this intermediate stage has been less documented in *D. salina* and may explain some of the confusion in the literature regarding the classification of reproductive stages. The retention of the mother cell membrane around daughter cells may also explain why early plasmolysis can be misinterpreted as aplanospore formation or dormancy.

Distinguishing Aplanospore Formation from Plasmolysis-Type Cell Death

Aplanospores are non-motile, resistant cells with a thickened cover that are produced under adverse conditions and can later germinate (Borowitzka & Siva 2007; Borowitzka 2018). In contrast, plasmolysis-type cell death is an irreversible process characterized by progressive

separation between the cell cover and the plasma membrane, cytoplasmic shrinkage, and loss of metabolic activity. Both processes involve cell rounding, loss of flagella, and sedimentation, making them difficult to distinguish without time-resolved observations or viability assays.

In our study, we used MTT reduction as a viability marker and observed that cells undergoing plasmolysis showed weak or negative MTT reduction. Furthermore, the onset of plasmolysis was consistently marked by an indentation at the cell surface, followed by progressive separation between the cell cover and the plasma membrane. This separation may initially be misinterpreted as thickening of the aplanospore wall or entry into a dormant phase. However, the presence of cytoplasmic shrinkage, surface indentation, membrane detachment, and loss of metabolic activity clearly distinguishes plasmolysis from aplanospore formation.

The Role of the Cell Cover and Plasma Membrane

D. salina lacks a rigid cell wall and is bounded by a glycoprotein-rich cell cover and an underlying plasma membrane. The functional connection between these two structures is essential for maintaining osmotic balance and cell shape. Under hypo-osmotic stress, the cell cover and plasma membrane may separate due to loss of functional proteins connecting them and failure of osmotic potential maintenance. This separation is a hallmark of plasmolysis-type cell death and should not be confused with the thickened cover of aplanospores or dormant cells.

Our observations suggest that the cell cover and plasma membrane are not only structurally distinct but also functionally independent during cytokinesis and stress responses. This has important implications for the interpretation of morphological data in Dunaliella and may help resolve some of the inconsistencies in the literature regarding the classification of reproductive and death stages. We consistently observed plasmolysis-type death (Fig. 5c) specifically within the sedimented cell fraction of aged laboratory cultures. This finding is critically linked to culture dynamics: as nutrients became depleted, the *D. salina* population entered a stationary and subsequent decline phase. Under such nutrient limitation, cells are known to undergo growth arrest and, in many microalgae, enter a state predisposing them to multiple fission or other survival strategies that often increase cell density and sedimentation. We posit that these sedimented, metabolically slowed cells face a compounded stress: the initial nutrient deprivation, coupled with potential hypoxia, waste accumulation, and altered signaling in the quiescent layer. In *D. salina*, which maintains osmotic balance in hypersaline environments via active ion transport and glycerol synthesis mediated by membrane protein kinases (Pick 2002; Wang et al. 2020), any sustained damage to these regulatory systems—whether from prolonged stress, oxidative damage, or yet-unknown factors inherent to the sediment microenvironment—could lead to a catastrophic failure of osmotic regulation. The resultant water loss and turgor pressure collapse would manifest as the observed detachment of the plasma membrane from the cell wall (plasmolysis), marking a terminal loss of cellular integrity.

Secretion-Type Death: A Consequence of Immobility and Microbial Fouling.

The secretion-type death (Fig. 5d), characterized by lipid droplet exudation and cell collapse, was exclusively found in heavily sedimented, old cultures. We propose five sequential mechanistic model for this phenomenon, linking physical immobilization to biotic attack:

1: Loss of Motility-Based Defense: In healthy, suspended cultures, the continuous flagellar beating of *D. salina* not only drives motility but also creates a fluid shear barrier, likely preventing the stable attachment of opportunistic bacteria and protozoan pathogens to the cell surface.

2: Environmental Viscosification: In aging cultures, the accumulation of exopolymeric substances (EPS) from the algal community itself increases the viscosity of the surrounding medium, particularly in the sediment layer (Xiao and Zheng 2016).

3: Immobilization and Attack: The increased viscosity severely impedes flagellar movement, effectively immobilizing the cells. This loss of mechanical defense allows surface-colonizing microbes to establish firm attachment and initiate biofilm-like formation on the algal cell (Fig. 5d1).

4: Breach of Integrity and Osmotic Collapse: The attached microbes likely secrete hydrolytic enzymes (e.g., algicides, cellulases, lipases) that degrade the protective glycocalyx and compromise the integrity of the cell wall and membrane, a process analogous to microbially-induced cell disruption described in algal systems (Demuez et al. 2015). This enzymatic attack creates pores, leading to a rapid disruption of osmotic equilibrium. The sudden influx of solutes or efflux of water causes extreme plasmolysis and physical crumpling of the cell.

5: Lipid Exudation: Concurrently, the internal turgor pressure collapse and membrane poration lead to the expulsion of cytoplasmic contents, most notably the lipid droplets that are characteristic of this death phenotype (Fig. 5d2-d3). This catastrophic release of intracellular lipids mirrors the desired outcome in biotechnological processes for algal lipid extraction via cell lysis (Lee et al. 2017). Thus, the observed process represents not merely passive lysis, but an active, though pathological, "secretion" driven by the internal pressure of the compromised cell under microbial siege.

A Practical Diagnostic Framework for Ecological Stress: Parallel MTT and Iodine Staining Reveals Dysfunctional Cell Death in Algae:

Our study introduces and validates a straightforward, yet powerful, morphological framework based on two parallel stains. By concurrently probing the two fundamental pillars of a photoautotroph's vitality—respiratory electron transport (via MTT) and photosynthetic carbon storage integrity (via iodine)—we move beyond simple viability assays to diagnose the functional

state leading to death. This methodological core provides a universal toolkit, as these metabolic and structural features are conserved across diverse algal taxa.

A critical insight from applying this toolkit is its inherent specificity for dysfunction. While it cannot, and does not claim to, catalog every conceivable death pathway, it reliably flags death arising from catastrophic failure in essential processes—whether induced by toxins (cisplatin), extreme photo-oxidation, osmotic collapse (plasmolysis), or biotic assault (secretion). This is its principal strength: distinguishing between regulated, physiological turnover and aberrant, stress-induced demise.

The framework's ecological relevance is powerfully demonstrated by its ability to detect spontaneous death phenotypes in environmental samples. We did not merely apply it to laboratory-induced stress; we employed it as a diagnostic lens on natural populations. The discovery of identical necrotic and plasmolysis signatures in cells from MHSW (Fig. 5b3, 5b) validates that the cell death pathways defined in the lab are operative in nature. Crucially, the method revealed previously overlooked death programs, such as the microbially facilitated 'secretion-type' death in aged cultures, underscoring its sensitivity for uncovering ecologically relevant mortality drivers that conventional assays might miss.

Therefore, the primary contribution of this work is not an exhaustive taxonomy of algal cell death, but the establishment of a robust, accessible, and interpretable diagnostic standard. However, this study was conducted using a single model species (*D. salina*), and therefore the general applicability of the proposed diagnostic framework across different algal taxa remains to be validated. Future work should extend this approach to a broader range of unicellular algae with varying cellular architectures and ecological niches to assess its robustness and universality. In addition, testing under diverse environmental stress conditions would further strengthen the applicability of this diagnostic standard in natural and applied systems, particularly for safeguarding cultures in photobioreactor systems, where early detection of population-level cell death could enable timely intervention and prevent the loss of valuable cultures.

Acknowledgments

We thank the Central Laboratory of Shiraz University of Medical Sciences for providing the Olympus BX61 microscope (operator: Dr. M. Mashhoody) and P. Elahi for graphical assistance, and we sincerely thank Dr. Matthew Davey (Scottish Association for Marine Science, Oban, UK) for his valuable editorial assistance and insightful comments on this manuscript.

Author Contributions Statement

Mahnaz Barmshuri: Conceptualization, Data curation, Formal analysis, Investigation, Methodology, Project administration, Software, Supervision, Validation, Visualization, Writing – review & editing
Saber Sadeghi: Investigation, Resources, Writing – review & editing
Bahman Kholdebarin: Supervision, Writing – review & editing
Zahra Faghih: Resources, Software
Laleh Ranjbaran: Methodology, Writing – review & editing

Disclosure statement:
No potential conflict of interest was reported by the authors.

Declaration of generative AI use:

During the preparation of this manuscript, the authors used DeepSeek and ChatGPT to improve the language and readability of the manuscript. The authors reviewed and edited all AI-generated content and take full responsibility for the final version of the manuscript.

Declaration of conflict of interest
The authors declare that they have no competing interests in relation to this work.

Statement of Informed Consent, Human/Animal Rights
No conflicts, informed consent, or human or animal rights are applicable to this study

Funding
No external funding was received for this study. The research was conducted without financial support from any funding agency, commercial organization, or not-for-profit institution.

References:

[1] Finkel, Z. V., Beardall, J., Flynn, K. J., Quigg, A., Rees, T. A. V., & Raven, J. A. (2010). Phytoplankton in a changing world: cell size and elemental stoichiometry. *Journal of plankton research*, *32*(1), 119-137. https://doi.org/10.1093/plankt/fbp098

[2] Bidle, K. D. (2015). The molecular ecophysiology of programmed cell death in marine phytoplankton. *Annual review of marine science*, *7*(1), 341-375. https://doi.org/10.1146/annurev-marine-010213-135014

[3] Segovia, M., Haramaty, L., Berges, J. A., & Falkowski, P. G. (2003). Cell death in the unicellular chlorophyte Dunaliella tertiolecta. A hypothesis on the evolution of apoptosis in higher plants and metazoans. *Plant physiology*, *132*(1), 99-105. https://doi.org/10.1104/pp.102.017129

[4] Franklin, D. J., Brussaard, C. P., & Berges, J. A. (2006). What is the role and nature of programmed cell death in phytoplankton ecology?. *European Journal of Phycology*, *41*(1), 1-14. https://doi.org/10.1080/09670260500505433

[5] Darehshouri, A., Affenzeller, M., & Lütz-Meindl, U. (2008). Cell death in the unicellular green alga Micrasterias upon H2O2 induction. *Plant biology (Stuttgart, Germany)*, *10*(6), 732. Plant Biology. htpp://doi.org/10.1111/j.1438-8677.2008.00078.x

[6] Jimenez, C., Capasso, J. M., Edelstein, C. L., Rivard, C. J., Lucia, S., Breusegem, S., ... & Segovia, M. (2009). Different ways to die: cell death modes of the unicellular chlorophyte Dunaliella viridis exposed to various environmental stresses are mediated by the caspase-like activity DEVDase. *Journal of experimental botany*, *60*(3), 815-828. https://doi.org/10.1093/jxb/ern330

[7] Yordanova, Z. P., Woltering, E. J., Kapchina-Toteva, V. M., & Iakimova, E. T. (2013). Mastoparan-induced programmed cell death in the unicellular alga Chlamydomonas reinhardtii. *Annals of Botany*, *111*(2), 191-205. https://doi.org/10.1093/aob/mcs264

[8] Gao, Y., & Erdner, D. L. (2022). Cell death responses to acute high light mediated by non-photochemical quenching in the dinoflagellate Karenia brevis. *Scientific Reports*, *12*(1), 14081. https://doi.org/10.1111/jeu.12874

[9] Gachon CM, Müller DG, Strittmatter M, Murúa P, Beckmann M, Tsirigoti A, Wawra S, Katsaros C, van West P, Küpper FC. Cell death is a conserved innate disease resistance response of brown algae against the oomycete Eurychasma dicksonii. iScience. 2025 Sep 19;28(9). https://doi.org/10.1016/j.isci.2025.113195

[10] Berman-Frank, I., Bidle, K. D., Haramaty, L., & Falkowski, P. G. (2004). The demise of the marine cyanobacterium, Trichodesmium spp., via an autocatalyzed cell death pathway. *Limnology and oceanography*, *49*(4), 997-1005. https://doi.org/10.4319/lo.2004.49.4.0997

[11] Murik, O., Elboher, A., & Kaplan, A. (2014). Dehydroascorbate: a possible surveillance molecule of oxidative stress and programmed cell death in the green alga C hlamydomonas reinhardtii. *New Phytologist*, *202*(2), 471-484. https://doi.org/10.1111/nph.12649

[12] Zamanpoore, M., Daremipouran, M. R., Ghaed-Abdi, M. R., & Ahmadi, N. K. (2019). Chemical and physical properties of Maharlu Salt Lake (Iran) prior to an extensive drought. *Ecopersia*, *7*(1), 59-67.

[13] Borowitzka, M. A., & Siva, C. J. (2007). The taxonomy of the genus Dunaliella (Chlorophyta, Dunaliellales) with emphasis on the marine and halophilic species. *Journal of Applied Phycology*, *19*(5), 567-590. https://doi.org/10.1007/s10811-007-9171-x

[14] Borowitzka, M. A. (2018). Biology of microalgae. In *Microalgae in health and disease prevention* (pp. 23-72). Academic Press. https://doi.org/10.1016/B978-0-12-811405-6.00003-7

[15] Xu, Y., Ibrahim, I. M., & Harvey, P. J. (2016). The influence of photoperiod and light intensity on the growth and photosynthesis of *Dunaliella salina* (chlorophyta) CCAP 19/30. *Plant Physiology and Biochemistry*, *106*, 305-315. https://doi.org/10.1016/j.plaphy.2016.05.021

[16] Ben-Amotz, A., Shaish, A., & Avron, M. (1989). Mode of action of the massively accumulated β-carotene of *Dunaliella bardawil* in protecting the alga against damage by excess irradiation. *Plant Physiology*, *91*(3), 1040-1043.https://doi.org/10.1104/pp.91.3.1040

[17] Kroemer, G., Galluzzi, L., Vandenabeele, P., Abrams, J., Alnemri, E. S., Baehrecke, E. H., ... & Melino, G. (2009). Classification of cell death: recommendations of the Nomenclature Committee on Cell Death 2009. *Cell death & differentiation*, *16*(1), 3-11. https://doi.org/10.1038/cdd.2008.150

[18] Bidle, K. D. (2016). Programmed cell death in unicellular phytoplankton. *Current Biology*, *26*(13), R594-R607. DOI: 10.1016/j.cub.2016.05.056

[19] Aguilera, A., Klemenčič, M., Sueldo, D. J., Rzymski, P., Giannuzzi, L., & Martin, M. V. (2021). Cell death in cyanobacteria: current understanding and recommendations for a consensus on its nomenclature. *Frontiers in Microbiology*, *12*, 631654. https://doi.org/10.3389/fmicb.2021.631654

[20] Ghasemi, M., Turnbull, T., Sebastian, S., & Kempson, I. (2021). The MTT assay: utility, limitations, pitfalls, and interpretation in bulk and single-cell analysis. *International journal of molecular sciences*, *22*(23), 12827. https://doi.org/10.3390/ijms222312827

[21] Carreno, E. A., Alberto, A. V. P., de Souza, C. A. M., de Mello, H. L., Henriques-Pons, A., & Anastacio Alves, L. (2021). Considerations and technical pitfalls in the employment of the MTT assay to evaluate photosensitizers for photodynamic therapy. *Applied Sciences*, *11*(6), 2603. https://doi.org/10.3390/app11062603

[22] Rosenzweig, E. S. F., Xu, B., Cuellar, L. K., Martinez-Sanchez, A., Schaffer, M., Strauss, M., ... & Jonikas, M. C. (2017). The eukaryotic CO2-concentrating organelle is liquid-like and exhibits dynamic reorganization. *Cell*, *171*(1), 148-162. DOI: 10.1016/j.cell.2017.08.008

[23] Barrett, J., Girr, P., & Mackinder, L. C. (2021). Pyrenoids: CO2-fixing phase separated liquid organelles. *Biochimica et Biophysica Acta (BBA)-Molecular Cell Research*, *1868*(5), 118949. https://doi.org/10.1016/j.bbamcr.2021.118949

[24] Galluzzi, L., Senovilla, L., Vitale, I., Michels, J., Martins, I., Kepp, O., ... & Kroemer, G. (2012). Molecular mechanisms of cisplatin resistance. *Oncogene*, *31*(15), 1869-1883. https://doi.org/10.1038/onc.2011.384

[25] Yang, Z., Schumaker, L. M., Egorin, M. J., Zuhowski, E. G., Guo, Z., & Cullen, K. J. (2006). Cisplatin preferentially binds mitochondrial DNA and voltage-dependent anion channel protein in the mitochondrial membrane of head and neck squamous cell carcinoma: possible role in apoptosis. *Clinical cancer research*, *12*(19), 5817-5825.

[26] Liu, J., Wang, Y., Qiao, P., Ying, Y., Lin, S., Lu, F., ... & Zhou, H. (2025). Mechanisms of Cisplatin-Induced Acute Kidney Injury: The Role of NRF2 in Mitochondrial Dysfunction and Metabolic Reprogramming. *Antioxidants*, *14*(7), 775. https://doi.org/10.3390/antiox14070775

[27] Brown, A., Kumar, S., & Tchounwou, P. B. (2019). Cisplatin-based chemotherapy of human cancers. *Journal of cancer science & therapy*, *11*(4), 97. PMID: 32148661

[28] Podratz, J. L., Knight, A. M., Ta, L. E., Staff, N. P., Gass, J. M., Genelin, K., ... & Windebank, A. J. (2011). Cisplatin induced mitochondrial DNA damage in dorsal root ganglion neurons. *Neurobiology of disease*, *41*(3), 661-668. https://doi.org/10.1016/j.nbd.2010.11.017

[29] Kleih, M., Böpple, K., Dong, M., Gaißler, A., Heine, S., Olayioye, M. A., ... & Essmann, F. (2019). Direct impact of cisplatin on mitochondria induces ROS production that dictates cell fate of ovarian cancer cells. *Cell death & disease*, *10*(11), 851. https://doi.org/10.1038/s41419-019-2081-4, DOI: 10.1016/j.cub.2016.05.057

[30] Orf, G. S., Gisriel, C. J., Granstrom, J., Baker, P. L., & Redding, K. E. (2022). The PshX subunit of the photochemical reaction center from Heliobacterium modesticaldum acts as a

low-energy antenna. *Photosynthesis research*, *151*(1), 11-30. https://doi.org/10.1007/s11120-009-9516-1

[31] Telfer, A. (2002). What is β–carotene doing in the photosystem II reaction centre?. *Philosophical Transactions of the Royal Society of London. Series B: Biological Sciences*, *357*(1426), 1431-1440. https://doi.org/10.1098/rstb.2002.1139

[32] Niyogi, K. K., & Truong, T. B. (2013). Evolution of flexible non-photochemical quenching mechanisms that regulate light harvesting in oxygenic photosynthesis. *Current opinion in plant biology*, *16*(3), 307-314. https://doi.org/10.1016/j.pbi.2013.03.011

[33] Dogra, V., & Kim, C. (2020). Singlet oxygen metabolism: from genesis to signaling. *Frontiers in plant science*, *10*, 1640. https://doi.org/10.3389/fpls.2019.01640

[34] Krieger-Liszkay, A., Fufezan, C., & Trebst, A. (2008). Singlet oxygen production in photosystem II and related protection mechanism. *Photosynthesis research*, *98*(1), 551-564. DOI:10.1023/A:1024969518145

[35] Exposito-Rodriguez, M., Laissue, P. P., Yvon-Durocher, G., Smirnoff, N., & Mullineaux, P. M. (2017). Photosynthesis-dependent H2O2 transfer from chloroplasts to nuclei provides a high-light signalling mechanism. *Nature communications*, *8*(1), 49. https://doi.org/10.1038/s41467-017-00074-w

[36] Kwiatkowski, S., Knap, B., Przystupski, D., Saczko, J., Kędzierska, E., Knap-Czop, K., ... & Kulbacka, J. (2018). Photodynamic therapy–mechanisms, photosensitizers and combinations. *Biomedicine & pharmacotherapy*, *106*, 1098-1107. https://doi.org/10.1016/j.biopha.2018.07.049

[37] Lan, M., Zhao, S., Liu, W., Lee, C. S., Zhang, W., & Wang, P. (2019). Photosensitizers for photodynamic therapy. *Advanced healthcare materials*, *8*(13), 1900132. https://doi.org/10.1002/adhm.201900132

[38] Orr, C. A. (2017). Warren JK: Evaporites: a geological compendium, 2nd edn.

[39] Krieger-Liszkay, A., Fufezan, C., & Trebst, A. (2008). Singlet oxygen production in photosystem II and related protection mechanism. *Photosynthesis research*, *98*(1), 551-564. DOI:10.1023/A:1024969518145

[40] Pick, U. (2002). Adaptation of the halotolerant alga Dunaliella to high salinity. In *Salinity: Environment-Plants-Molecules* (pp. 97-112). Dordrecht: Springer Netherlands. https://doi.org/10.1007/0-306-48155-3_5

[41] Wang, M., Chen, S., Zhou, W., Yuan, W., & Wang, D. (2020). Algal cell lysis by bacteria: a review and comparison to conventional methods. *Algal Research*, *46*, 101794. https://doi.org/10.1016/j.algal.2020.101794

[42] Xiao, R., & Zheng, Y. (2016). Overview of microalgal extracellular polymeric substances (EPS) and their applications. *Biotechnology advances*, *34*(7), 1225-1244. https://doi.org/10.1016/j.biotechadv.2016.08.004

[43] Demuez, M., González-Fernández, C., & Ballesteros, M. (2015). Algicidal microorganisms and secreted algicides: new tools to induce microalgal cell disruption. *Biotechnology Advances*, *33*(8), 1615-1625. https://doi.org/10.1016/j.biotechadv.2015.08.003

[44] Lee, S. Y., Cho, J. M., Chang, Y. K., & Oh, Y. K. (2017). Cell disruption and lipid extraction for microalgal biorefineries: A review. *Bioresource technology*, *244*, 1317-1328. https://doi.org/10.1016/j.biortech.2017.06.038